Search for New and Unusual Stangeonia States Using $\gamma p \to p\phi\eta$ with GlueX at Thomas Jefferson National Accelerator Facility

Prospectus of Dissertation

Bradford E. Cannon
Department of Physics, Florida State University

March 25, 2016

Major Professor:	Dr. Paul Eugenio	_____
Committee Member:	Dr. Volker Crede	_____
Committee Member:	Dr. Simon Capstick	_____
Committee Member:	Dr. Ettore Aldrovandi	_____
Committee Member:	Dr. Horst Wahl	_____

Abstract

I propose to search for new and unusual strangeonium states produced in the reaction $\gamma p \to p\phi\eta$. The data used for this analysis will come from Hall D of Thomas Jefferson National Accelerator Facility, where the GlueX experiment is located. The GlueX experiment will use a linearly polarized coherent bremsstrahlung beam of up to 12 GeV in energy. This photon beam will interact with a stationary liquid hydrogen target located inside the GlueX detector. The subsequent photoproduction will provide final states ideal for studying both exotic and non-exotic $s\bar{s}$ mesons. Preliminary Monte Carlo analysis of this reaction will be provided and will show an expected acceptance of 0.04279 for a detected proton, and an acceptance of 0.09795 for a missing proton. Further analysis will need to be done on the collected data and Monte Carlo to identify the presence of $s\bar{s}$ resonances. Additionally, it may be necessary to perform a partial wave analysis. This analysis will help to determine the presence of both excited $s\bar{s}$ resonances and exotic J^{PC} $s\bar{s}$ states.

1 Introduction

One of the most important questions in all of particle physics is "what is matter made of?" That is to say, what are the fundamental building blocks for which all things are comprised of. This question dates all the way back to ancient Greece where philosophers postulated the existence of an atom; or something that is indivisible. This idea resonated throughout time with the eventual discovery of protons, neutrons, and electrons which are the building blocks of the periodic table of the elements. However, in the 1900's [1], particles with electric charge other than the proton and electron were discovered. Since these particles have masses between the proton and electron, they were described as mesons, or 'middle weights'. The number of discovered mesons continued to grow which led to physicists wonder if there were different fundamental building blocks of matter other than the proton, neutron, and electron. This question would eventually be answered with the creation of the Eightfold Way by Murray Gell-Mann circa 1961 [2].

Gell-Man introduced a way of organizing all of the known mesons and baryons into groups that shared patterns of strangeness, charge, and isospin. These diagrams helped to show that hadronic matter is comprised of six different quarks and anti quarks which are held together by their interaction via the strong nuclear force. Examples of baryon and meson multiplets are depicted in Figure 1 below [3].

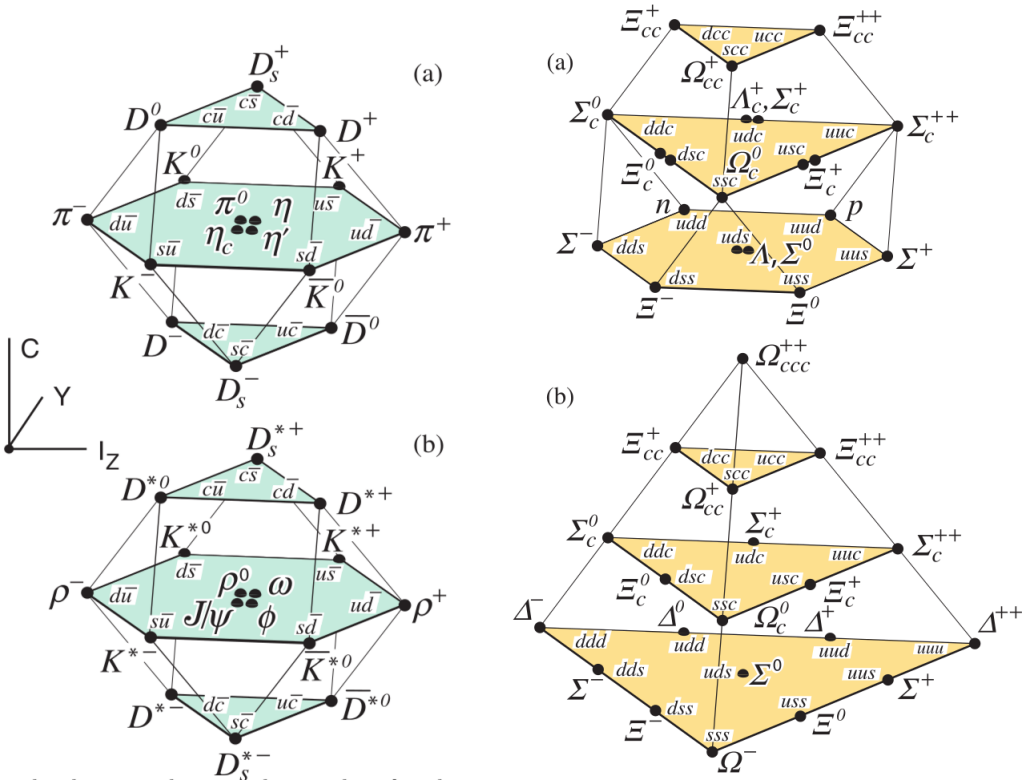

Figure 1: (upper-left) $J^{PC} = 0^{-+}$ pseudoscalar meson multiplet. (upper-right) $J^{PC} = 1/2^+$ baryon multiplet. (lower-left) $J^{PC} = 1^{--}$ vector meson multiplet. (lower-right) $J^{PC} = 3/2^+$ baryon multiplet

The strong nuclear force is described by Quantum Chromodynamics (QCD), which is a theory that predicts the behaviour of particles that couple to the color field. These particles include all quarks, antiquarks, and gluons which are the quantized mediators of the strong force. Quarks, anti-quarks, and gluons have similar characteristics of other well known particles. These characteristics

include mass, electromagnetic charge, and quantum numbers such as spin and angular momentum. When a quark and an anti quark are in a bound state (ie - a meson) their individual quantum numbers combine to make a total bound state with a given J^{PC}.

Knowing that a quark and antiquark have spin 1/2, it is easy to investigate the possible quantum numbers of all $q\bar{q}$ mesons, regardless of quark/antiquark flavor. A table of good quantum numbers for all mesons is given below.

$$constraints : |l - s| <= J <= |l + s|, P = (-1)^{l+1}, C = (-1)^{l+s}$$

s	$l = 0$	$l = 1$	$l = 2$
$s = 0$	0^{-+}	1^{+-}	2^{-+}
$s = 1$	1^{--}	0^{++},1^{++},2^{++}	1^{--},2^{--},3^{--}

If you take a closer look at the resulting J^{PC} states in the table above, you should notice that certain states are missing; such as 0^{--}, 0^{+-}, 1^{-+}, and 2^{+-}. These states are known as exotic J^{PC} meson states. In addition to exotic J^{PC} meson states, QCD allows the existance of other exotic states such as $q\bar{q}q\bar{q}$ (four quark), $qqqq\bar{q}$ (pentaquark), and $q\bar{q}g$.

2 Motivation

To date, there are no universally accepted non $q\bar{q}$ meson states; only observed exotic meson candidates. The primary reason for this is the absence of an established $q\bar{q}$g nonet. The purpose of the GlueX experiment at Jefferson Lab is to unambiguously map exotic meson states. In order to establish exotic nonets, we need to first understand non exotic meson states. An example of a non exotic state that is poorly understood is $s\bar{s}$ strangeonia.

Out of the twenty-two expected $s\bar{s}$ resonances below 2.2 GeV, only seven probable resonances exist : $\eta\eta'$, $\phi(1020)$, $h_1(1386)$, $f_1(1426)$, $f_2'(1525)$, $\phi(1680)$, and $\phi_3(1386)$; where I am counting $\eta\eta'$ as one resonance [4]. Of these seven resonances, only three of them are considered pure $s\bar{s}$ states : $\phi(1020)$ $f_2'(1525)$, and $\phi_3(1386)$. Due to the heavy nature of the strange quark in comparison to the up and down quarks, one would expect more pure $s\bar{s}$ states to exist in nature.

Historically, there has been some controversy over the identification of $s\bar{s}$ states in the 1600-2200 MeV mass range; specifically the $\phi(1680)$, $X(1750)$, and $Y(2175)$ meson states. The first observation of $\phi(1680)$ came from the DM1 collaboration at DCI in 1981. The experiment analysed the $K_s^o K_L^o$ final state and observed an enhancement in the cross section between 1.6-1.8 GeV center of mass energy [5]. This enhancement was eventually observed to have a dominant decay into a neutral KK^* final state. An odd feature of the $\phi(1680)$ is that it has only been observed in electron-positron annihilation experiments, and has not been observed in photoproduction.

Six months after the discovery of $\phi(1680)$, the X(1750) meson was observed by the Omega Photon collaboration at CERN [6]. The experiment analysed a K^+K^- final state from photoproduction and found a clear enhancement in the invariant mass spectrum of the K^+K^- pair. It is not clear whether this state is unique or simply a shift of the $\phi(1680)$ mass due to the tail of a vector meson nearby in mass. It should also be noted that photoproduction studies of this final state have shown no evidence of a resonance at 1680 MeV.

Lastly, the BaBar collaboration at SLAC discovered a structure at 2175 MeV in the reaction $e^+e^- \to \phi f_0(980) \to K^+K^-\pi\pi$ [7]. The $K^+K^-\pi\pi$ final state invariant mass distribution showed a clear enhancement around 2175 GeV. Due to the fact that the structure came from a $\phi f_0(980)$ intermediate state, it has been suggested that this is a 1^{--} four quark strageonium hybrid state [8].

The underlying issue with all of the observations previously described is that the production of final state kaons does not necessarily confirm the existence of an $s\bar{s}$ state. The only way to ensure that a state has $s\bar{s}$ content is to choose an intermediate state in which the parent $u\bar{u}$ / $d\bar{d}$ content is suppressed. One channel that will resolve this ambiguity is $\phi\eta$. If a state is shown to have a significant branching fraction to $\phi\eta$, it will be good evidence that the state is an $s\bar{s}$ state. Furthermore, if a state is not seen in the $\phi\eta$ channel, it will be good evidence that the state has little to no $s\bar{s}$ content. The reason for this will be described in more detail below.

3 Proposed Analysis

The purpose of this research is to accomplish at least one out of two goals. The first is to provide a spectrum of excited s$\bar{s}$ states using the $\phi\eta$ channel. The $\phi\eta$ channel is a unique final state to study because it can only be produced from a parent state that is dominantly comprised of s$\bar{s}$ quarks. The reason for this is due to two different characteristics of the $\phi\eta$ final state. One characteristic is due to the fact that the ϕ meson is almost pure $s\bar{s}$. The second characteristic is that the $\phi\eta$ channel is OZI suppressed for $u\bar{u}$ and $d\bar{d}$ final states. Example Feynman diagrams for the $s\bar{s}$ and OZI suppressed $\phi\eta$ final states are given in Figure 2 below.

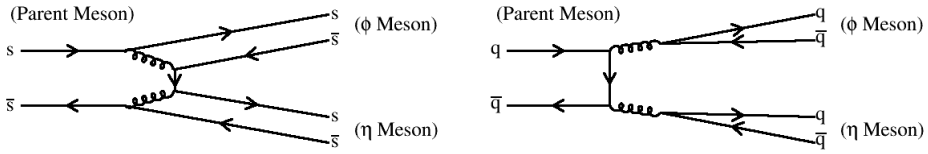

Figure 2: (left) Feynman Diagram depicting the decay of a parent $s\bar{s}$ state into $\phi\eta$ strangeonia. (right) Feynman Diagram depicting the decay of an arbitrary $q\bar{q}$ parent state into $\phi\eta$ quarkonia.

As previously stated, an observation of a parent state that has a large branching fraction to $\phi\eta$ will be good evidence of a dominant $s\bar{s}$ excited state. Conversely, if there is an absence of a state in $\phi\eta$, it should have little to no $s\bar{s}$ content. Understanding and establishing dominant s$\bar{s}$ states is an important aspect to meson spectroscopy because there are only three well known states to date; the $\phi(1020)$, the $f_2^{'}(1525)$, and the $\phi_3(1854)$.

The second goal of this research will be to search for exotic mesons using the $\phi\eta$ channel. Knowing that the ϕ meson has $J^{PC} = 1^{--}$, and that the η meson has $J^{PC} = 0^{-+}$, it is easy to derive what parent states can produce $\phi\eta$ with different relative angular momentums. A table of possible parent states is given below.

l	J^{PC}
$l = 0$	1^{+-}
$l = 1$	0^{--}, 1^{--}, 2^{--}
$l = 2$	1^{+-}, 2^{+-}, 3^{+-}

There are three states above that are of particular interest, the most obvious being the 0^{--} and the 2^{+-}, since they are inherently J^{PC} exotic. The other state of interest is the 2^{--} since it is not well understood.

4 GlueX

CEBAF

CEBAF is an acronym which stands for Continuous Electron Beam Accelerator Facility. The beam is created by injecting slow moving electrons into a linear accelerator where they are given enough energy to enter the 7/8 mile accelerator track which is located at Jefferson Lab. This horse race track shaped accelerator increases the velocity of the electrons by using electrically charged chambers inside the straight regions of the oval track. When the electrons are leaving the straight portion of the accelerator track, the beam is split into five different tracks located inside the curved region of the accelerator. These five different tracks hold bunches of electrons with different energies. Once the beam is split, all five portions of the beam now enter the curved region where large magnets are placed in order to bend the path of the electrically charged particles. The accelerator facility has recently been upgraded to provide three experimental halls at Jefferson Lab with 11 GeV of energy, and a new hall at 12 GeV. At this energy, the beam line will deliver bunches of electrons into the experimental halls every four nanoseconds.

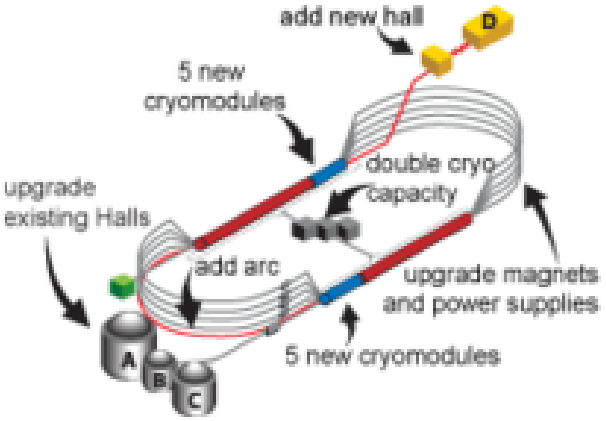

Figure 3: Illustration of the accelerator track and the experimental halls located at JLab.

Diamond Radiator

There are four different experimental halls at Jefferson Lab; Hall A, Hall B, Hall C, and Hall D. Halls A, B, and C are located at the south-west section of the accelerator oval, whereas Hall D is located unaccompanied at the opposite end of the accelerator oval. When electrons are approaching the direction of Halls A, B, and C, they can either continue straight into those halls or continue around the track towards Hall D. Once inside the Hall D, the beam collides into a Diamond Radiator. Interaction with the radiator produces coherent Bremsstrahlung radiation which acts as the photon beam in Hall D. The diamond radiator is a 3 micron wide plane that can change its orientation relative to the beam direction adjusted. These orientation adjustments allow GlueX to control the energy of the radiation as well as the orientation of its polarization. Knowing the polarization of the incident photons will allow GlueX to study photon-proton interactions as a function of the photon polarization.

Photon Beam

Once the linearly polarized photon beam is created by the diamond radiator, it continues straight towards the GlueX detector. Before reaching Hall D, the beam travels through a series collimators which only allow photons travelling with a particular direction to pass. This reduces the amount of noise from the Bremsstrahlung radiation and ensures that the beam is travelling towards the proton target. In addition, the scattered electrons that are left over from the interaction with the diamond radiator are bent by a magnetic field and are ejected towards a tagger which measures their energy. Knowing the initial energy of the incident electron beam, and then measuring the recoiled energy of the electrons allows us to get an idea of the energy of the photons that are about to enter Hall D.

We also use an additional detector farther down stream called the pair spectrometer. The main purpose of the pair spectrometer is to measure the photon flux incident collimated beam. It can also be used to measure the beam energy and polarization. When a photon enters the pair spectrometer, it can interact with a radiator which produces an electron-positron pair. When this charged lepton pair is created, their path is immediately deflected due to the magnetic field of the pair spectrometer. The particles eventually collide with scintillators which record the electron-positron hits. Knowing the radiation length of the radiator and the amount of hits in the pair spectrometer per unit time allows us to measure the incident photon flux. Additionally, measuring the energy of the electron-positron pair allows us to determine the energy of the incident beam.

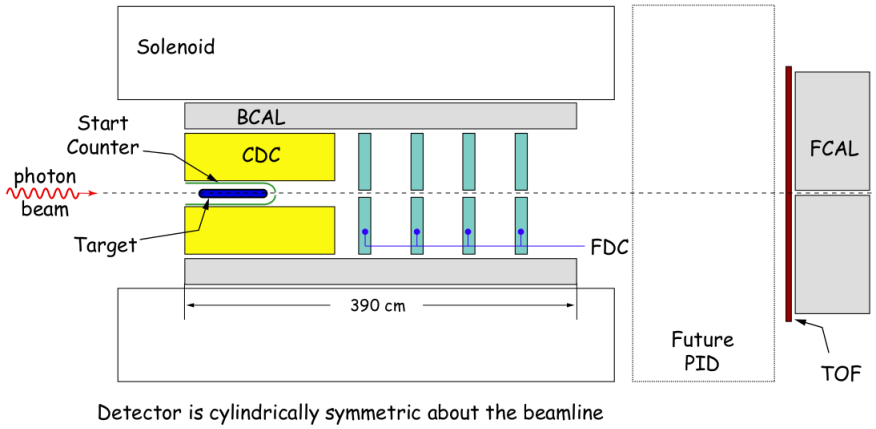

Figure 4: Depiction of the GlueX detector at JLab.

Target

Once the photon beam enters the GlueX detector, it will then interact with the target. The target is a long cylindrical chamber of that is filled with liquid Hydrogen (LH_2). The target is aligned in the direction of the photon beam in order to increase the likelihood of observing an interaction with one of the protons at rest.

Start Counter

The start counter is the first detector located outside of the target chamber. The purpose of the start counter is to record the time of the photon-proton interaction. Since photon beam bunches arrive in Hall D every four nanoseconds, it is important to identify which bunch is responsible for the proton interaction taking place so GlueX can perform accurate particle identification. Currently, the start counter has a resolution of 0.28 nano seconds.

Superconducting Solenoid/Magnet

The superconducting solenoid/magnet is the most outer part of the barrel portion of the GlueX detector. The purpose of the superconducting solenoid/magnet is to produce a magnetic field responsible for bending charged particles inside the detector. The existence of this magnetic field allows us to determine both the charge of a particle as well as its momentum. The momentum of a charged particle is proportional to the radius of curvature around a magnetic field line.

Central Drift Chamber

The central drift chamber (CDC) is a large cylindrical detector that is 1.5m long and has an inner radius of 10 cm and an outer radius of 54cm. The CDC is positioned inside the GlueX detector such that it is wrapped around the start counter and only extends 1.5m in the beam line direction. Located inside the central drift chamber is a series of straw tubes which are filled with gas and wires that point in a direction parallel to the beam line. When a charged particle travels trough the central drift chamber it will ionize the gas inside the straw tubes. This allows an amplified electrical pulse to be carried down a wire where the signal can be collected. This characteristic allows the CDC to measure the path of charged particles and also the amount of energy deposited into the gas as a function of distance.

Forward Drift Chambers

The forward drift chambers (FDC) are located downstream of the central drift chamber and are encapsulated by the superconducting solenoid/magnet and barrel calorimeter. The purpose of the FDC is to measure the tracks of charged particles ejected in the forward going region. It consists of 24 one-meter-diameter chambers with both wire and cathode readouts. A gas sits between the cathode readout chambers so that a charged particle track will radiate when passing through the detector. The FDC readouts therefore operate in a similar fashion to the CDC, such that when a charged particle passes through the material, an electrical amplification is collected and a measurement is made. Finally, the FDC specializes in reconstructing high density charged particle tracks.

Barrel Calorimeter

The barrel calorimeter (BCAL) is another cylindrically shaped object that is 3.9 meters long, with an inner radius of 64.3 cm and an outer radius of 90.5 cm. The purpose of the barrel calorimeter is to measure the energy of particles, especially photons. The BCAL is comprised of thin layers of lead sheets with scintillating wires that run through them; parallel to the direction of the beam. When a particle enters the BCAL, it excites several electrons inside the scintillation material, which then radiate energy in the form of photons. The photons travel down the scintillation wires until they reach the endpoints of the barrel where they are then collected by light guides which then leads to photo multiplier tubes (PMT). The PMT's collect the light signals and convert them into amplified electrical pulses.

Forward Calorimeter

The detector that is located farthest downstream in GlueX is called the Forward Calorimeter. Much like the Barrel Calorimeter mentioned before, the purpose of the Forward Calorimeter is to measure the energy of neutral particles travelling in the forward direction. The Forward calorimeter is comprised of 2800 modules that contain a lead bar connected to an optical cookie and photomultiplier tube. When a neutral particle interacts with the lead blocks, all of the energy is absorbed and detected by the optical cookie and photomultiplier tube.

Time-of-Flight

Unlike the aforementioned detectors, the time of flight (TOF) is square in shape and is 3m x 3m in size. The time of flight is located downstream of the cylindrical portion of the GlueX detector and is before the forward calorimeter. The time of flight is comprised of transparent scintillating bars that are wrapped in highly reflective material so that no light can escape. The scintillation material in the TOF is similar to the scintillation material in the BCAL. When a particle hits the TOF, the electrons inside the scintillation material become excited and radiate photons which travel down the material and are eventually collected by a PMT. The purpose of the time of flight is to deduce how long it took a particle to travel from the interaction vertex (start counter) to the TOF detector. Since the distance travelled of the particle is known from the drift chamber paths (for charged particles), we can divide this by the time to calculate a velocity. Knowing the momentum of the charged particle from the radius of curvature about the magnetic field, we can divide the momentum by the velocity and calculate a mass. This allows us to identify different particle species inside the GlueX detector.

5 Preliminary Monte Carlo Analysis

This section will include two different sets of analyses. One of them will consider the reaction $\gamma p \to p\phi\eta$ with a detected proton, and the other analysis will consider the reaction $\gamma p \to [p]\phi\eta$ with a missing proton. The purpose of investigating these two reactions is to study the quality of acceptance inside the GlueX detector as a function of proton detection. To begin these analyses 100,000 events were generated using a Monte Carlo technique which produced the $pK^+K^-\gamma_1\gamma_2$ final state. The Monte Carlo technique generates these events by specifying a reaction in consecutive decay steps described below.

1. Specify that the beam is a photon at 9 GeV
2. Specify that the target is a proton at rest
3. Make the proton a final state particle
4. Declare an unknown parent state for the ϕ and η mesons
5. Demand that the ϕ meson decays into a K^+K^- pair
6. Demand that the η meson decays into a $\gamma_1\gamma_2$ pair

The Monte Carlo procedure is designed such that it automatically conserves four momentum and also decays particles uniformly in all directions, relative to their parent rest frames. Knowing these angular distributions allows us to understand the reconstruction efficiencies for the GlueX detector which will be discussed later. After the final state four momentums are generated, they are then passed into a GlueX detector simulation program. This simulation program takes the four momentums as input, and then outputs a corresponding Hall D data file. The output data file contains timing and hit information for all of the sub detectors inside GlueX. Once this information is outputted, it is then 'smeared' in order to match the resolution of the sub detectors.

The final file with sub detector timing and hit information will then be passed into a simulation reconstruction program. The simulation reconstruction program is instructed to search for events that contain hit and timing information consistent with the final state that you wish to study. It is here where the two different analysis channels, $\gamma p \to p\phi\eta$ and $\gamma p \to [p]\phi\eta$, will produce different

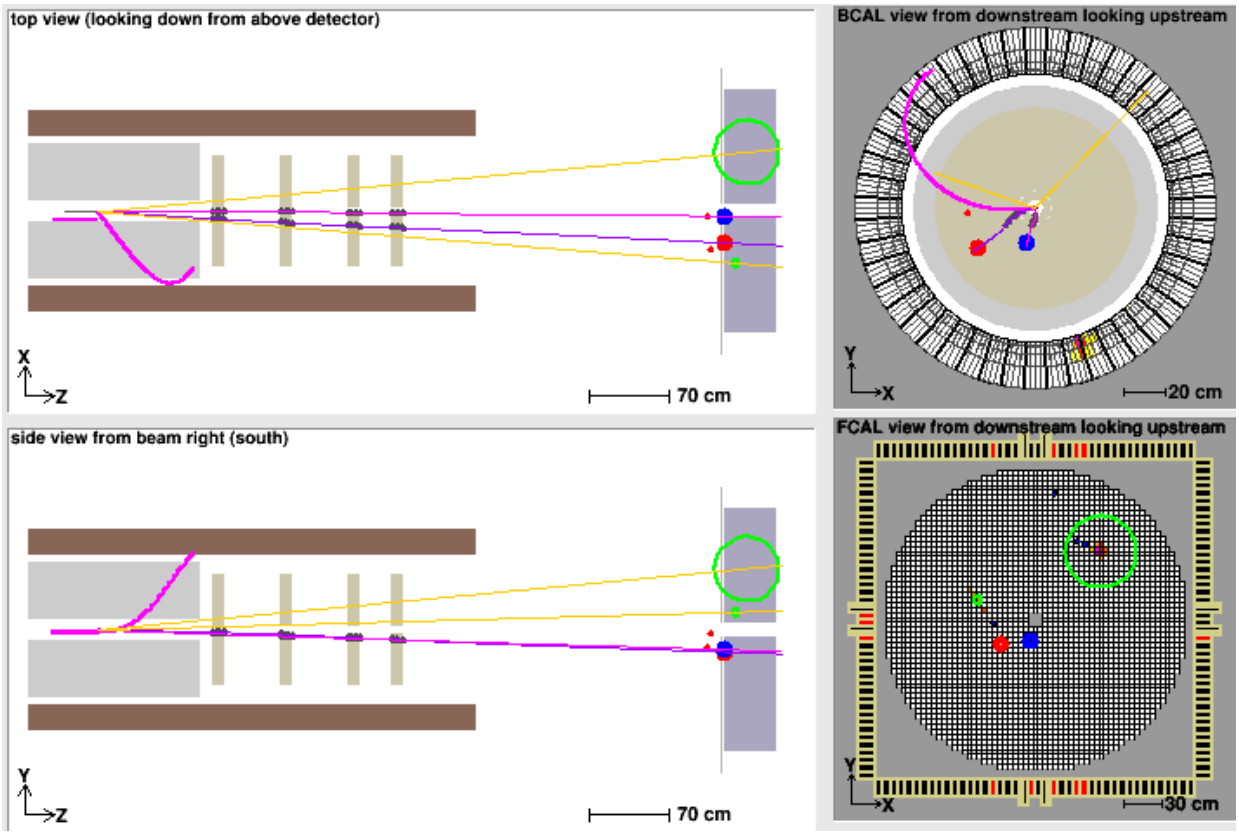

Figure 5: Example of a reconstructed Monte Carlo event with three charged tracks and two neutral tracks. The light purple track that passes through the CDC is a low momentum proton, while the other two forward going charged tracks are K^+ and K^- originating from a ϕ meson. The two straight yellow lines are the reconstructed photon tracks from the η assuming they originated from inside the target chamber. If you look closely you can see the hit signals inside the FDC from the kaons as well as the hits for the photons and kaons inside the TOF and FCal. Hits inside the CDC were present as well for the proton but were emitted from the image for the purpose of track clarity.

results. One one hand, the channel with the detected proton will demand to see at least two positive tracks, while the channel with the missing proton will only demand to see one positive track. Additionally, both channels will require at least two neutral showers from the photons, as well as at least one negatively charged track for the K^-.

Once the simulation reconstruction has only allowed these events to pass, it will then assign hypotheses to all positive and negative tracks. For the positive tracks it will assume the track came from e^+, π^+, K^+, and protons; while for the negative tracks it assumes e^-, π^-, and K^-. Since this analysis is only interested in $\phi\eta$, only the hypothesis that contain kaons and protons will be collected. Once the desired final state has been collected, cuts can be made on the accepted Monte Carlo. To begin, it is required that the invariant mass for $\gamma_1\gamma_2$ be near the η mass. Another requirement is the invariant mass of the K^+K^- pair to be near the ϕ mass. Examples of these invariant mass distributions and their cuts are given in Figure 6 below.

Some additional cuts can be made on the missing mass and energy. For the system with the detected proton this is very easy, simply require that the missing invariant mass and energy be near zero. However, for the reaction with the missing proton we are only allowed to cut on the missing invariant mass and not the missing energy since the four momentum of the missing proton

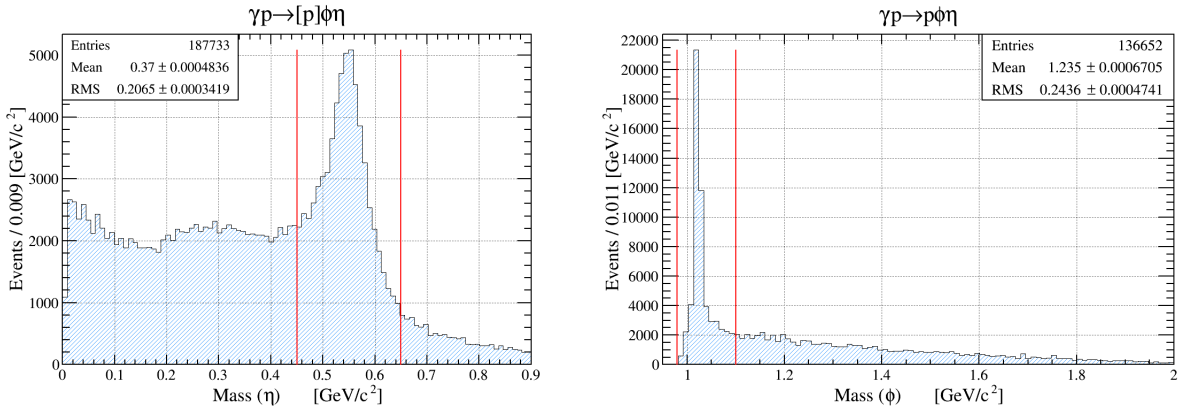

Figure 6: (left) The invariant mass distribution of the reconstructed $\gamma_1\gamma_2$ four vectors. The vertical red lines in the figure denote where the cut on the invariant mass is made in order to select an η meson. (right) The invariant mass distribution of the reconstructed K^+K^- four vectors. The vertical red lines in the figure denote where the cut on the invariant mass is made in order to select a ϕ meson.

is unknown. An example of a missing energy cut and a missing invariant mass cut is given in Figure 7 below.

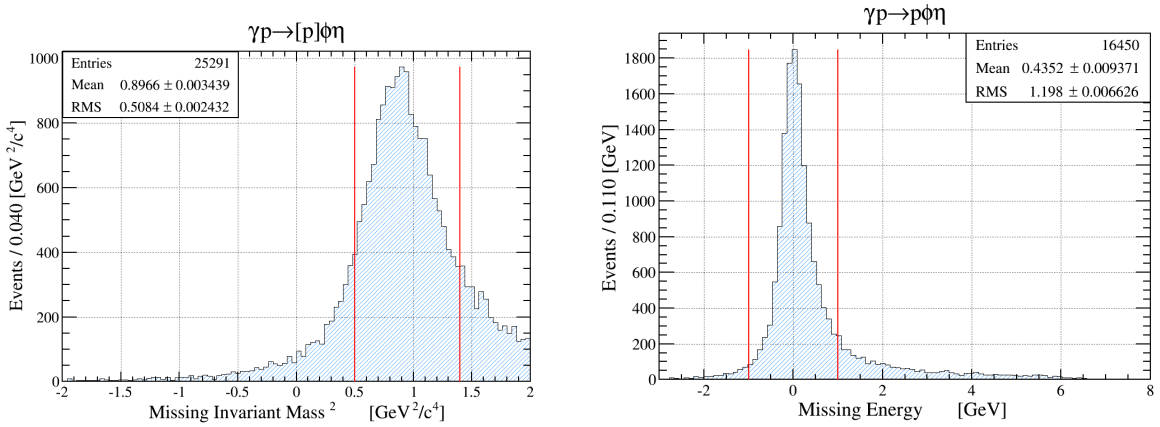

Figure 7: (left) Invariant mass distribution of missing mass. This is calculated by taking the square of the measured initial state and final state four vectors $m^2_{mm} = [\gamma_\mu + p_\mu - (K^+_\mu + K^-_\mu + \gamma_{1,\mu} + \gamma_{2,\mu})]^2$. (right) Missing energy distribution with a detected proton. This is calculated by subtracting the sum of all final state energies from the initial state energies $E_{miss} = \gamma_o + p_o - (p_o + K^+_o + K^-_o + \gamma_{1,o} + \gamma_{2,o})$

Another important aspect of this analysis is to differentiate between protons and positively charged kaons. One way that we can do this at GlueX is by looking at the amount of energy lost in the Central Drift Chamber (CDC) per unit of distance. At low momentums, the protons typically lose more energy in the CDC as compared to the kaons. Since the momentum and the energy loss in the CDC are two measurements we can perform at GlueX, we can plot them against each other on a two dimensional color histogram to both investigate this behaviour and impose cuts. An example of an observed proton and K^+ spectra with cuts are given in Figure 8 below.

Lastly, one can also differentiate between protons and positively charged kaons by comparing their measured β values as a function of momentum. Due to the differences in invariant mass between the two particles, it is possible to make particle identification cuts in this way. For the

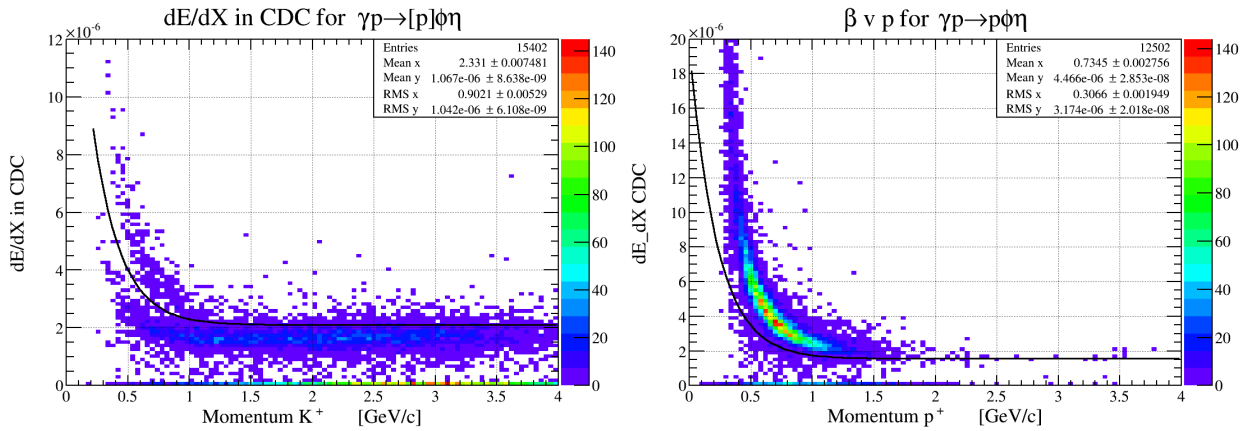

Figure 8: (left) Two dimensional color histogram of energy loss in the CDC per unit distance (vertical axis) versus the measured momentum inside the CDC (horizontal axis) of positively charged tracks. The black line is the cut being made in order to differentiate between protons at low momentum. (right) Another two dimensional color histogram of energy loss in the CDC per unit distance versus the measured momentum inside the CDC of positively charged tracks. The black line is the cut being made in order to differentiate between kaons at low momentum.

protons, this cut will be imposed by shifting the function $\left|\overrightarrow{P}\right| / \sqrt{m_i^2 + \left|\overrightarrow{P}\right|^2}$ horizontally, while for the kaons the function will be shifted vertically. Examples of β vs. $\left|\overrightarrow{P}\right|$ plots with cut lines for protons and positively charged kaons are given in Figure 9 below.

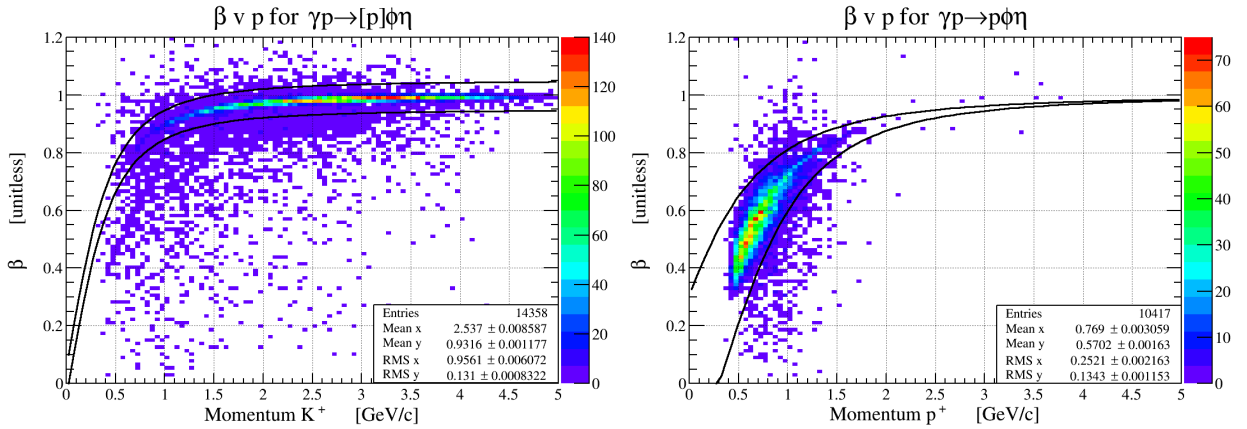

Figure 9: (left) Two dimensional color histogram of measured $\beta = v/c$ (vertical axis) versus the measured momentum (horizontal axis) of positively charged tracks. The black lines are the cuts being made in order to select positively charged kaons. (right) Another two dimensional color histogram of measured $\beta = v/c$ versus the measured momentum of positively charged tracks. The black lines are the cuts being made in order to select protons.

Now that the kaon and proton signals have been separated, it is important to investigate the acceptance for each analysis in order to determine which will yield more statistics for actual data. In principal, acceptance is a function of several different observables. However, for the purpose of this preliminary analysis, acceptance will be defined as the number of events that survived all of the cuts mentioned above divided by the total number of initial events that were generated (100,000).

After this analysis, an acceptance of 0.04279 was found for a detected proton, and an acceptance of 0.09795 was found for a missing proton. An additional study of acceptance can be done by looking at the invariant mass distribution of ϕ and η for the generated and accepted Monte Carlo. Example distributions with calculated acceptances for both the detected proton and missing proton channels are provided in Figure 10 below.

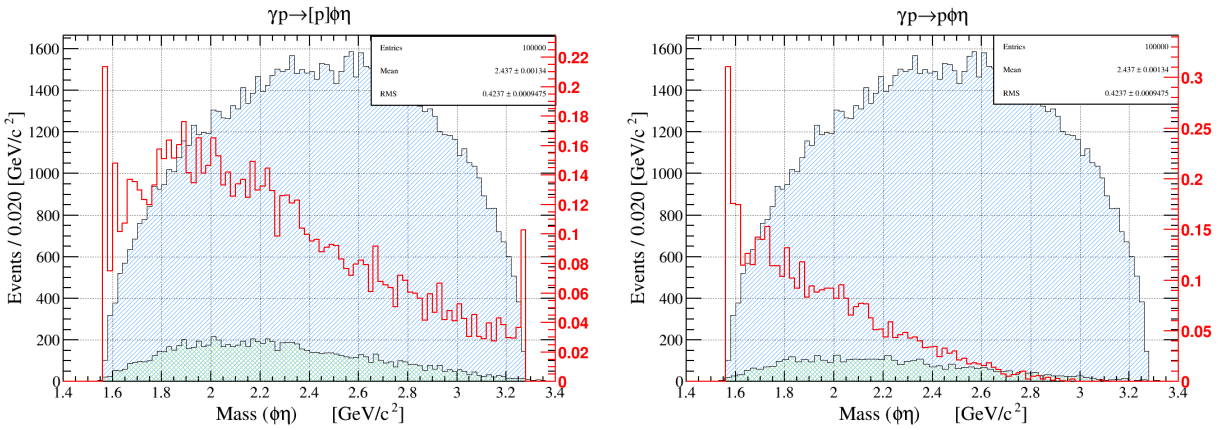

Figure 10: (left) Acceptance distribution for the invariant mass of selected $\phi\eta$ events with a missing proton. The green histogram bars represent the accepted Monte Carlo events after cuts. The blue histogram bars represent the of generated Monte Carlo events. The red line represents the calculated bin by bin acceptance. This is calculated by dividing the number of accepted Monte Carlo events per bin, by the number of generated Monte Carlo events per bin. (right) Acceptance distribution for the invariant mass of selected $\phi\eta$ events with a detected proton.

6 Future Analysis

Clearly there is much more analysis that needs to be done with $\gamma p \to p\phi\eta$. Some of these future analyses plans include understanding the background associated with the GlueX experiment as well as collecting real data to perform analysis on. In order to perform these necessary steps, it is also important to optimize the simulation reconstruction routines at GlueX, which is an on going effort. Finally, when these steps are accomplished, a partial wave analysis may be performed on the data set. This analysis will allow us to see which wave sets contribute to the overall signal observed in my channel.

7 References

[1] Griffiths, G. C. D. Introduction. Springer Netherlands, 1972.

[2] Gell-Mann, Murray. The eightfold way: A theory of strong interaction symmetry. No. TID-12608; CTSL-20. California Inst. of Tech., Pasadena. Synchrotron Lab., 1961.

[3] K.A. Olive et al. (Particle Data Group), Chin. Phys. C, 38, 090001 (2014).

[4] Barnes, T., N. Black, and P. R. Page. "Strong decays of strange quarkonia." Physical Review D 68.5 (2003): 054014.

[5] F. Mané et al. (DM1), Phys. Lett. 99B, 261 (1981).

[6] D. Aston et al. (Omega Photon), Phys. Lett. 104B, 231 (1981).

[7] Aubert, Bernard, et al. "Structure at 2175 MeV in $e^+e \to \phi f_o(980)$ observed via initial-state radiation." Physical Review D 74.9 (2006): 091103.

[8] A Candidate for 1– strangeonium hybrid - Ding, Gui-Jun et al. Phys.Lett. B650 (2007) 390-400 hep-ph/0611319 USTC-ICTS-06-14